Technical Report

TR-2009-009

Mathematical and Numerical Modeling of Focal Cerebral Ischemia

by

E. Agostoni, M. Perego, S. Salsa, A. Veneziani

Mathematics and Computer Science

EMORY UNIVERSITY

Mathematical and numerical modeling of focal cerebral ischemia

Elio Agostoni* Mauro Perego† Sandro Salsa‡
Alessandro Veneziani§

March 19, 2009

Abstract

Cerebral focal ischemia is a local degeneration of brain tissue induced by a reduction of blood supply. We introduce a mathematical model that includes the blood dynamics, represented by a flow in a porous medium and ion dynamics (calcium and potassium), together with other variables (energy stores, tissue integrity, oxygen and glucose) representing the biochemical events consequent to the vessel occlusion. The accurate description of the coupling between fluid dynamics and Biochemics is one of the distinctive features of the present work. We present both 2D and 3D simulations. Occurrence of peculiar ion dynamics, called *spreading depression* waves, formerly pointed out in the literature, is observed in 2D results. The role of some parameters of the problem in suppressing these waves is discussed. We moreover simulate in 3D the effects of a forced reperfusion of the occluded vessel (*fibrinolysis*) and the consequent blood leakage (*hemorrhagic infarct*).

1 Introduction

Cerebral focal ischemia is a localized degeneration of brain tissue induced by a reduction of blood and oxygen supply. Tissue damage can be partially or totally recovered in the so called *ischemic penumbra* while the core of the degeneration, where the damage is not reversible, is called *ischemic umbra* (see [11]). Biochemical mechanisms of degeneration still need a deep investigation in view of the set up of appropriate therapies. The pharmacological

*Neuroscience Department, A. Manzoni Hospital, Lecco, Italy

†MOX (Modeling and Scientific Computing), Dipartimento di Matematica "F. Brioschi",Politecnico di Milano, Italy; ref. address: mauro.perego@polimi.it

‡Dipartimento di Matematica "F. Brioschi",Politecnico di Milano, Italy

§Department of Mathematics and Computer Science, Emory university, Atlanta, Georgia

elimination of blood supply reduction (typically a vascular occlusion), called *fibrinolysis* is quite often unfeasible since it can induce a dramatic hemorrhage. Mathematical and numerical models can provide a paradigm for a deep comprehension of these phenomena (see [33, 29, 32, 15, 31, 13]). The main difficulties in this context rely on:

(i) intrinsic complexity of the phenomena at hand, involving interacting fluid and biochemical dynamics; this typically reflects into complexities of the associated mathematical models, given by systems partial and ordinary differential and sometimes algebraic equations;

(ii) complexity of the geometries at hand that can play a relevant role (see [14]);

(iii) parameters identification and evaluation (see [13, 35]).

These difficulties affect the set up of reliable numerical models. Numerical simulations in the literature in this field are so far limited to 2D geometries, involving different biochemical dynamics. In particular, in [29, 33, 8] the role of the *spreading depression* (SD) in the penumbra tissue degeneration is emphasized, while a global overview of different possible mechanisms involved, including the effects of glutamate, is discussed in [13]. In [12] a detailed description of the calcium dynamics is reported, while the possible role of geometry in the SD waves is analyzed in [14]. In all these works, the role of the hemodynamics is lumped into an average parameter describing the Cerebral Blood Flow (CBF) for the district at hand in terms of an ordinary differential (see [33]) or an algebraic (see [13]) equation.

The aim of the present work is twofold. On one hand, following the guidelines of the models proposed in [33, 35, 9] including dynamics for intra and extra cellular potassium and calcium ions and of some heuristic indexes for the tissue integrity and the metabolic stores, we devise a rigorous model for the ions dynamics and include a precise description of the fluid dynamics. More precisely, by means of "average volume" techniques (see [37, 25, 28]), we present a model accounting for local dynamics in an average way, giving a mesoscale picture of the physiopathology in brain circulation, basically referring to cortical spreading depression models. Cortical spreading depression was firstly studied by Leão [26] in 1944. It as a localized depression of neural activity that spreads through the tissue. It has been correlated with migraine aura and with ischemia. In [18] cortical spreading depression phenomenon was detected in injured human brain. The hypothesis that SD can be generated by ischemic events was investigated by means of mathematical models in [33, 29]. Here we essentially move from these works, and we set up a model with a strong physical motivation. Moreover, we include a space dependent description of the blood dynamics assuming that the vascular tissue can be regarded as a porous medium. To this aim, we replace the

ordinary differential equation of the flow in the original model of [33] with the Darcy law for porous media. Our basic idea is that the permeability is a function of the integrity of the tissue. The more precise formulation of the hemodynamics will eventually allow to simulate of the action of fibrinolytic therapies and their possible failures.

The second goal is to extend numerical simulations of the phenomena at hand in 3D computationss, with an ad hoc finite element code. Numerical results presented here show at a qualitative level dynamics that can be induced by the combination of biochemical events following the stroke and the reperfusion of the occluded vessels. The quantitative validation of the model used here requires and adequate collection of experimental data. This represents an important development of the present work.

The outline of the paper is as follows. Section 2 is devoted to the presentation of the mathematical model. By means of volume averaging technique, models for the biochemical and the blood dynamics are introduced separately. The coupled model is presented at the end of the section.

Sect. 3 is devoted to the numerical discretization. Space discretization is carried out by means of the finite element method and time discretization is obtained by classical finite difference schemes. The linearization of the model is obtained by an appropriate explicit-in-time treatment of the nonlinear terms. The development of the code for this problem has been carried out within the framework of the C++ Object Oriented `LifeV` library (see [2]). In Section 4 we present and comment numerical simulations. Conclusions and perspectives are drawn in Sect. 5.

1.1 Basic Notations

Let Ω be a bounded domain in $\mathbb{R}^d$ ($d = 2, 3$). With usual notation, we denote by $L^2(\Omega)$ the space of real functions whose square is integrable in Ω and by $(\cdot, \cdot)$ and $\| \cdot \|$ the associated inner product and norm, respectively. The corresponding vector space $(L^2(\Omega))^d$ will be denoted by $\mathbf{L}^2(\Omega)$. Similarly, we introduce the space $H^1(\Omega) = \{v \in L^2(\Omega) | \nabla v \in \mathbf{L}^2(\Omega)\}$ whose norm is denoted $\| \cdot \|_1$. Correspondingly, we set $\mathbf{H}^1(\Omega) = (H^1(\Omega))^d$ and we still denote its norm by $\| \cdot \|_1$.

1.1.1 Volume average

In order to describe how microscale dynamics affect mesoscale phenomena we carry out *volume averaging* (see [6] and [37] for more details). For a given (scalar, vector, tensor) function ψ, the volume average will be denoted by:

$$< \psi > (\mathbf{x}_B) = \frac{1}{|\Omega|} \int_{\Omega_f(\mathbf{x}_B)} \psi(\mathbf{x}) \, d\Omega \tag{1}$$

where for a region Ω with centre of mass in $\mathbf{x}_B$, $\Omega_f(\mathbf{x}_B) \subset \Omega$ represents the domain of ψ. $|\Omega|$ denotes the measure of $\Omega(\mathbf{x})$, that is assumed to be constant for each $\mathbf{x}_B$.

The mesoscale region Ω where we carry out the space average is called REV (*Reference Element of Volume*). *Porosity* is defined as:

$$n_f = \frac{|\Omega_f|}{|\Omega|}. \tag{2}$$

We call *homogeneous* a medium with constant porosity. We also denote the *intrinsic volume average* by $< \psi >_f = \frac{|\Omega|}{|\Omega_f|} < \psi >$. The following result (valid for homogeneous media) will be extensively used in the sequel (see [6]):

$$< \operatorname{div} \psi >_f = \operatorname{div} < \psi >_f + \frac{1}{|\Omega_f|} \int_{A_I} \psi \cdot \mathbf{n} d\Omega \tag{3}$$

where A_I is the boundary of Ω_f inner to Ω and $\mathbf{n}$ is the normal unit vector outward to A_I.

In particular, in our model a generic domain Ω features two main subregions, the Blood Domain and the Tissue Space separated by the *Blood Brain Barrier* (BBB). The latter is in turn split into two subdomains, namely the Intracellular Space (ICS) and the Extracellular Space (ECS). We refer to the Blood Domain, the Tissue Space, the ICS and the ECS with the subscripts b, t, i and e, so that

$$\Omega = \Omega_b \cup \Omega_t = \Omega_b \cup \Omega_i \cup \Omega_e.$$

Volume average in the respective regions will be denoted by $< \cdot >_b, < \cdot >_t, < \cdot >_i, < \cdot >_e$ and the associated porosity by n_b, n_t, n_i, n_e.

2 The mathematical model

Focal ischemia and cerebral infarct are the consequence of dynamics involving mainly (1) blood in arteries, capillaries and veins; (2) ions in the cells and the extra-cellular space. These dynamics drive the evolution of energy stores and other tissue properties. In this Section we provide a mesoscale representation of these dynamics, by performing volume average on a volume with small vessels, extra-cellular and intra-cellular space, such that at the end they will be not distinguished anymore in the final model (see Fig. 1). Largest vessels of the brain will be considered external to the domain of interest. We retain a space dependence accurate enough to account local phenomena such as the blood leakage associated to the cerebral infarct.

For the sake of clarity, we address the hemodynamics and the ion dynamics seprately.

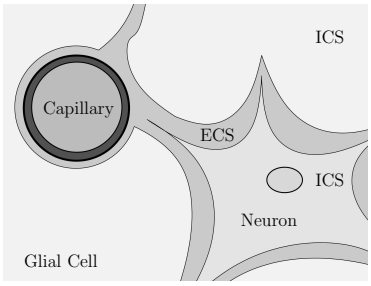

Figure 1: Extracellular space, intracellular space and capillary

2.1 Cerebral hemodynamics

As previously pointed out, in our domain we assume the brain be composed by three subdomains, *capillaries*, *extracellular space* and *intracellular space*. Cells membranes and capillaries walls will be assumed to be rigid for the sake of simplicity. Large vessels act as appropriate boundary condition for the problem. Compliance of walls and membranes and auto-regulation of the cerebral circulation are neglected, even if their appropriate modeling represents a development of the present work. We will also neglect rheological effects of blood, so that blood will be assumed to be a Newtonian fluid.

The basic idea is to consider at the mesoscale the brain as a porous medium for the blood. Macroscopic dynamics of a fluid in a filled porous medium can be described by means of the well known *Darcy Law* (see [6], [37]):

$$\mathbf{q} = -\mathbf{K}\ \nabla\phi_b \tag{4}$$

where $\mathbf{q} =< \mathbf{v} >$ is the average velocity of blood, $\phi_b =< \phi >_b$ the blood average pressure and $\mathbf{K}$ is the hydraulic conducibility tensor. Here we assume that the brain is an isotropic homogeneous material, so that $\mathbf{K} = \mu\mathbf{I}$ where $\mathbf{I}$ is the identity tensor and we can write $\mathbf{q} = -\mu\nabla\phi_b$. Since the walls are assumed to be rigid and the fluid is incompressible, $\operatorname{div}\mathbf{q} = 0$, so that a possible model for hemodynamics reads

$$\begin{cases} -\operatorname{div}(\mu\ \nabla\phi_b) = 0 & \text{in } Q_T = (0,T)\times\Omega \\ \phi_b = \varphi(\mathbf{x},t) & \text{on } \Sigma_D = [0,T]\times\Gamma_D \\ -\mu\ \nabla\phi_b\cdot\mathbf{n} = \eta(\mathbf{x},t) & \text{on } \Sigma_N = [0,T]\times\Gamma_N \end{cases} \tag{5}$$

where $\Omega(\subset\mathcal{R}^3)$ is the space domain and $\Gamma_D\cup\Gamma_N = \partial\Omega$, $\varphi(\mathbf{x},t)$ and $\eta(\mathbf{x},t)$ are given functions.

Here $\mathbf{q}$ is an average blood velocity including both venous and arterial blood. Several work address how to properly describe the different type of blood depending on the vessel type (artery, capillary, vein). More precisely,

hierarchical porous media theory ([24, 36, 10]) allows to associate a suitable conductivity tensor with each vessel type solving a system of Darcy like equations. In this paper, for the sake of simplicity we do not distinguish the different vessels in (5). However it is possible to get an approximate estimate of blood velocity in arterial, capillaries and venules, once computed ϕ_b with (5), by the simple approximation

$$\mathbf{q}_a \simeq -\mu_a \nabla \phi_b, \quad \mathbf{q}_c \simeq -\mu_c \nabla \phi_b, \quad \mathbf{q}_v \simeq -\mu_v \nabla \phi_b.$$

where μ_a, μ_c and μ_v are the conductivities of the three subdomains respectively. This estimate is derived under the rough assumption that arterioles and venules blood velocities have the same direction, that yields conductivities be proportional to the average vessel lengths and $\mu_a + \mu_c + \mu_v = \mu$.

Remark 2.1 *It is possible to introduce vessel compliance by means of a time derivative term in the first equation of system (5), see [6]. We get rid this term here since blood transitories are fast compared to ischemia dynamics.*

2.2 Biochemical dynamics

Ions dynamics in ECS and ICS are driven by thermal diffusion and electrical field. Since the potential differences are relevant only across the cell membranes (see [9]), we get rid of the latter term. A complete description of diffusion in brain tissue can be found in [28].

To fix the ideas, let us refer to the extracellular space. We denote with X both the ion and its concentration. By applying the volume average (1) to mass conservation of ion X, featuring diffusion coefficient D_X and unit flux $\mathbf{J}_X$, we get

$$< \frac{\partial X}{\partial t} >_e = - < \operatorname{div} \mathbf{J}_X >_e = -\operatorname{div} < \mathbf{J}_X >_e - \frac{1}{|\Omega_e|} \int_M \mathbf{J}_X \cdot \mathbf{n} \, d\sigma, \qquad (6)$$

where M is the interface between ECS and ICS and between ECS and blood. Since the ionic exchanges between the ECS and the blood are small and slow (see [35]), we get rid of the interface ECS-blood. Following [25], we will assume that the Fick law in the porous medium can be written as:

$$< \mathbf{J}_X >_e = -D_X \, \mathbf{T} \, \nabla < X >_e \qquad (7)$$

where $\mathbf{T}$ is a symmetric positive definite tensor. More precisely in isotropic media, $\mathbf{T} = \lambda^{-2}\mathbf{I}$ where the *tortuosity* parameter λ is in general ≥ 1 and represents the resistance to the diffusion of the ion at hand in a free space versus the one in a porous media. In the cerebral extracellular space, we have $\lambda_e \in [1.5, 1.8]$. It is worth observing that although (7) holds only for fluxes

$\mathbf{J}_X$ that have a linear dependence on ionic concentrations, nevertheless the Fick law is often assumed to be realistic with general fluxes ([28]).

Let us denote by $J_X = -\mathbf{J}_X \cdot \mathbf{n}$ the ionic flux outgoing from ICS to ECS. From (6) and (7) we get:

$$\frac{\partial < X >_e}{\partial t} = \frac{D_X}{\lambda_e^2} \triangle < X >_e + \frac{|M|}{|\Omega_e|} \, J_X. \tag{8}$$

Similarly, for the ICS we have:

$$\frac{\partial < X >_i}{\partial t} = \frac{D_X}{\lambda_i^2} \triangle < X >_i - \frac{|M|}{|\Omega_i|} J_X \tag{9}$$

In the latter equations, the thickness of the membrane M has been neglected. For the sake of notation, in the sequel we set $\alpha_e = \frac{|M|}{|\Omega_e|}$ e $\alpha_i = \frac{|M|}{|\Omega_i|}$.

2.2.1 The ionic model

Following the Tuckwell and Miura model ([35]) for the Cortical Spread Depression, we consider the simplified model involving potassium and calcium ions. The former features high concentration and high impact on the cytoplasmic membrane potential, thanks to its high permeability. The latter influences the potassium permeability and has an important role in the ischemic pathology. In the sequel we denote by K_e (resp. K_i) and Ca_e (resp. Ca_i) the ECS (resp. ICS) potassium and calcium concentrations. Equations (8, 9) read (for the easiness of notation we drop the average symbol $<>$)

$$\begin{cases} \dfrac{\partial K_e}{\partial t} = \dfrac{D_K}{\lambda_e^2} \triangle K_e + \alpha_e \, J_K \\ \dfrac{\partial K_i}{\partial t} = \dfrac{D_K}{\lambda_i^2} \triangle K_i - \alpha_i \, J_K \\ \dfrac{\partial Ca_e}{\partial t} = \dfrac{D_{Ca}}{\lambda_e^2} \triangle Ca_e + \alpha_e \, J_{Ca} \\ \dfrac{\partial Ca_i}{\partial t} = \dfrac{D_{Ca}}{\lambda_i^2} \triangle Ca_i - \alpha_i \, J_{Ca} \end{cases} \tag{10}$$

Ionic fluxes result from the balance of dynamics induced by ionic gradients (passive flux J_K^p) and the action of active pumps (J_K^a), so that

$$J_K = J_K^a + J_K^p, \quad J_{Ca} = J_{Ca}^a + J_{Ca}^p. \tag{11}$$

Following [35] we have:

$$\begin{aligned}
J_K^a &= -f_K(1-\exp^{r_K(K_e^0-K_e)}) - J_K^0,\\
J_{Ca}^a &= f_{Ca}(1-\exp^{r_{Ca}(Ca_i^0-Ca_i)}) - J_{Ca}^0,\\
J_K^p &= -p_K g_0(1+\tanh(p_g(V+V_g)))(V-V_{Ca})(V-V_K),\\
J_{Ca}^p &= g_0(1+\tanh(p_g(V+V_g)))(V-V_{Ca}),\\
V &= V_{th}\ln\frac{K_e+\gamma}{K_i+\delta}, \quad V_K = V_{th}\ln\frac{K_e}{K_i}, \quad V_{Ca} = V_{th}\ln\frac{Ca_e}{Ca_i},
\end{aligned} \tag{12}$$

where V, V_K, V_{Ca} are the membrane potential, the potassium and calcium Nernst potentials respectively and $V_{th} = \frac{RT}{F}$ is the thermal voltage, being R the Boltzman constant (8.314 [J mol^{-1} K^{-1}]), F the Faraday constant (96.485 [C mol^{-1}]) and T the absolute temperature.

In [35], ions diffusion in ICS is neglected ($\lambda_i = \infty$). However, presence of possible neurons junctions allowing ions diffusion in ICS is described in [34]. For a recent analysis of these approaches, see [27].

2.2.2 Brain tissue metabolism

Active pumps J_K^a, J_{Ca}^a depend on brain tissue metabolism and hemodynamics. Most of cell energy is stored in ATP molecule. ATP is mostly synthesized through oxidative phosphorylation in normoxic conditions and by anaerobic glycolysis during hypoxia ([16]). The ATP moles per unit volume in the tissue, representing the energy store, are denoted hereafter by E. If P_{ATP} denotes the ATP synthesized per unit time and Q_{ATP} the ATP consumption per unit time, we have

$$\frac{\partial E}{\partial t} = P_{ATP} - Q_{ATP}. \tag{13}$$

In the brain, about $40\% - 60\%$ of ATP production is used to maintain ion gradients [16], consequently, we model ATP consumption as

$$Q_{ATP} = c_{ATP}\ \alpha_t J^a + \frac{E}{E+E_{cr}} c_Q.$$

The first term on the right hand side represents the consumption related to active fluxes through the cell membrane, while c_Q is the (constant) basal consumption of the tissue. When $E = E_{cr}$ the basal consumption is halved.

The total ATP demand R_{ATP} can be defined as

$$R_{ATP} = Q_{ATP} + \frac{(E^0 - E)}{\tau_E}$$

where E^0 is the physiological resting value of the energy store E, and τ_E is a time constant. The rightmost term acts to limiting fluctuations in energy stores.

Accurate description of ATP production requires appropriate models for Oxygen partial pressure and glucose concentration. In normoxic conditions 1 mole of glucose and 6 moles of oxygen yields 36-38 moles of ATP, while anaerobic glycolysis yields only 2 moles of ATP by a mole of glucose [16]. ATP production $[mM\ min^{-1}]$ (where $[M] \equiv [mol\ dm^{-3}]$) is given therefore by:

$$P_{ATP} = 2Q_G^{an} + 6Q_O,$$

where Q_G^{an} and Q_O are the anaerobic consumption of glucose and oxygen respectively. Referring to Roos and Sperber in [32] and [31], we assume Oxygen consumption to be described by *Hill* dynamics, depending on oxygen partial pressure in tissue (P_t) and glucose concentration in tissue (G_t), namely

$$Q_O = \frac{1}{6} R_{ATP} \frac{P_t}{P_t + K_O} \frac{G_t}{G_t + K_G},$$

being K_O and K_G the dissociation constants for oxygen and glucose. In physiological conditions $G_t >> K_G$, then Q_O is almost independent on small variation in G_t. To maintain the basal energy supply, even in hypoxic condition[32], anaerobic consumption of glucose reads

$$Q_G^{an} = \frac{1}{2} R_{ATP} \left(1 - \frac{P_t}{P_t + K_O}\right) \frac{G_t}{G_t + K_G}$$

When glucose concentration is high enough (i.e. $Q_G >> K_G$), the ATP production P_{ATP} is almost equal to the ATP demand R_{ATP}. Total glucose consumption Q_G is given by

$$Q_G = Q_G^{an} + \frac{Q_O}{6}.$$

since in aerobic synthesis of ATP, one molecule of glucose reacts with 6 molecules of oxygen.

In blood a small fraction of oxygen is dissolved in plasma, being the remaining part bound to Hemoglobin molecules. We denote by O_p and O_{Hb} the concentrations of the two fractions of oxygen respectively. At equilibrium the saturation rate of Hemoglobin f_{Hb} is a function of dissolved Oxygen O_p that can be approximated by the *Hill* equation [5]:

$$f_{Hb}(O_p) = \frac{O_p^h}{O_p^h + \overline{O}_p^h}$$

being h the so called *Hill* exponent that we assume $h = 3$, and $\overline{O_p}$ the Oxygen corresponding to $f_{Hb} = \frac{1}{2}$. Since each molecule of Hemoglobin

binds 4 oxygen molecules, given the concentration of Hemoglobin Hb, we have that:

$$O_{Hb} = 4Hb f_{Hb}(O_p). \tag{14}$$

We consider the former identity to hold even in the non stationary case since the characteristic time of the reaction is only $\tau_r \simeq 5s$. Since only the dissolved oxygen can pass through the blood brain barrier, oxygen concentration in blood will obey the Advection-Reaction-Diffusion equation:

$$\frac{\partial(O_p + O_{Hb})}{\partial t} - \frac{D_O}{\lambda_b^2}\triangle O_p + \frac{1}{n_b}\mathbf{q}\cdot\nabla(O_p + O_{Hb}) + \beta_b c_O(O_p - O_t) = 0,$$

being D_O the constant effective diffusion of dissolved oxygen in the blood, O_t the oxygen in the tissue, β_b (see Table 1) a coefficient stemming from usual average procedures. Constant c_O is defined as $c_O = D_O/d$, where d is the membrane thickness. In defining c_O we are assuming the Fick law to hold in the Blood Brain Barrier (BBB). Diffusion of O_{Hb} can be considered negligible (see [19]).

Exploiting (14) we obtain:

$$\chi(O_p)\frac{\partial O_p}{\partial t} - \frac{D_O}{\lambda_b^2}\triangle O_p + \frac{\chi(O_p)}{n_b}\,\mathbf{q}\cdot\nabla O_p + \beta_b c_O(O_p - O_t) = 0.$$

being $\chi(O_p) = 1 + 4Hb\, f'_{Hb}(O_p)$. When the chemical at hand is a gas, it is more appropriate to write the equation in term of partial pressure of the gas in the solution than in term of the concentration. The equation of the partial pressure of the oxygen $P_b = \frac{O_p}{\sigma_b}$, being σ_b the solubility of oxygen in blood, reads

$$\chi(\sigma_b P_b)\frac{\partial P_b}{\partial t} - \frac{D_O}{\lambda_b^2}\triangle P_b + \frac{\chi(\sigma_b P_b)}{n_b}\,\mathbf{q}\cdot\nabla P_b + \beta_b c_O(P_b - \frac{\sigma_t}{\sigma_b}P_t) = 0, \tag{15}$$

where $P_t = \frac{O_t}{\sigma_t}$ and σ_t is the solubility of oxygen in tissue. Correspondingly, the partial pressure of the oxygen in tissue fulfills the equation:

$$\frac{\partial P_t}{\partial t} - \frac{D_O}{\lambda_t^2}\triangle P_t + \beta_t c_O(P_t - \frac{\sigma_b}{\sigma_t}P_b) + \frac{1}{\sigma_t}Q_O(P_t, G_t) = 0. \tag{16}$$

Remark 2.2 *Parameter c_O plays a major role (see [20]). With the assumption of very high permeability of membrane ($c_O \to \infty$) we have $\sigma_b P_b \simeq \sigma_t P_t$ and we can reduce (15) and (16) to*

$$\left[\beta_b + \beta_t\chi(\sigma_b P_b)\right]\frac{\partial P_t}{\partial t} - D_O\left(\frac{\beta_b}{\lambda_t^2} + \frac{\beta_t}{\lambda_b^2}\right)\triangle P_t + \frac{\beta_t}{n_b}\chi(\sigma_t P_t)\,\mathbf{q}\cdot\nabla P_t + \tfrac{\beta_b}{\sigma_t}Q_O(P_t, G_t) = 0.$$

After similar considerations, for the glucose concentrations in blood (G_b) and in tissue (G_t) we have

$$\begin{cases} \dfrac{\partial G_b}{\partial t} - \dfrac{D_G}{\lambda_b^2}\triangle G_b + \dfrac{1}{n_b}\mathbf{q}\cdot\nabla(G_b) + \beta_b c_G\left(\dfrac{G_b}{G_b+\overline{K}_G} - \dfrac{G_t}{G_t+\overline{K}_G}\right) = 0, \\ \dfrac{\partial G_t}{\partial t} - \dfrac{D_G}{\lambda_e^2}\triangle G_t + \beta_t c_G\left(\dfrac{G_t}{G_t+\overline{K}_G} - \dfrac{G_b}{G_b+\overline{K}_G}\right) + Q_G(P_t, G_t) = 0. \end{cases} \tag{17}$$

Unlike Oxygen, glucose cannot diffuse through the BBB and the cell membrane. Transport of glucose through the membrane is performed by specific carriers. Reactions term in previous equations has been proposed by Robinson and Rapoport [30]. Tortuosity λ_e is basically tortuosity of the ECS, since glucose cannot diffuse through the cells.

2.2.3 Tissue impairment

Tissue integrity I is an empirical index measuring the tissue health introduced in [29]. For $I = 1$ we have an intact tissue, while $I = 0$ corresponds to necrosis. Dynamics of I are based on the following assumptions. I is reduced when the energy store E is below the critical threshold E_{cr} and when the calcium concentration in the ICS is over a critical value Ca_{cr}. We have therefore:

$$\frac{\partial I}{\partial t} = -\left(c_{IE}(E_{cr}-E)^+ + c_{ICa}(Ca_i - Ca_{cr})^+\right) I \tag{18}$$

where with $(\,\cdot\,)^+$ we indicate the positive part of the argument; in particular, $(E_{cr}-E)^+$ is defined as:

$$(E_{cr}-E)^+ = \begin{cases} 0 & \text{if} \quad E \geq E_{cr} \\ E_{cr}-E & \text{if} \quad E < E_{cr} \end{cases}.$$

Note that I is never increasing, which implies that tissue impairment cannot be recovered. Physiological ionic fluxes are described by (12). Extension to this model including possible pathologies account of the following dynamics:

1. ionic pumps reduce their action when E decrease and when the tissue is impaired;
2. ionic fluxes across the cytoplasmic membrane are enhanced when I decreases.

Consequently, generalization of (12) reads

$$J_K^a = -I\,\frac{E}{E+E_{cr}}\left[f_K(1-\exp^{\,r_K(K_e^0-K_e)}) + J_K^0\right]$$
$$J_{Ca}^a = I\,\frac{E}{E+E_{cr}}\left[f_{Ca}(1-\exp^{\,r_{Ca}(Ca_i^0-Ca_i)}) - J_{Ca}^0\right]$$
$$J_K^p = -[1+c_{JK}\,(I_{cr}-I)^+]p_K g_0(1+\tanh[p_g(V+V_g)])(V-V_{Ca})(V-V_K)$$
$$J_{Ca}^p = [1+c_{JC}\,(I_{cr}-I)^+]g_0(1+\tanh[p_g(V+V_g)])(V-V_{Ca})$$

Effect of tissue impairment on hemodynamics It has been found [22, 21] that tissue impairment will increase BBB permeability. This clearly affects the blood dynamics. As a matter of fact, at the mesoscale we generalize model (5) by assuming that a blood flow external to the vessel could be induced by the increased BBB permeability (γ). More precisely, we assume

$$\begin{cases} -\text{div}\,(\mu\ \nabla\phi_b) = \gamma(I)\dfrac{M_{bt}}{|\Omega|}(\phi_t - \phi_b) \\ -\text{div}\,(\tilde{\mu}\ \nabla\phi_t) = \gamma(I)\dfrac{M_{bt}}{|\Omega|}(\phi_b - \phi_t) \end{cases} \tag{19}$$

where M_{bt} is the surface area of the BBB in the REV and $\tilde{\mu}$ the hydraulic conductivity of the tissue space. When $I = 1$ we have $\gamma(I) = 0$ and $\phi_t = 0$. When $\gamma(I)$ increases ($\gamma(I) \to \infty$), we have that $\phi_b \simeq \phi_t$ and we can reduce equations (19) to

$$-\text{div}\ ((\mu + \tilde{\mu})\ \nabla\phi_b) = 0.$$

This argument illustrates that the effect of tissue impairment can be modeled as an increment of the hydraulic conductivity for in (5). More precisely, we assume

$$\mu = [1 + c_{nb}\,(I_{cr} - I)^+]\mu_0 \tag{20}$$

where μ_0 is the physiological value of hydraulic conductivity and c_{nb} is an empirical coefficient.

2.3 The complete model

The complete model coupling hemodynamics and biochemical dynamics is given therefore by (5) with (10), (13), (15), (16), (17) and (18). The equations are completed by suitable boundary and initial conditions.

The problem is well defined when the ionic variables (K_e, K_i, Ca_e, Ca_i) are bounded and strictly positive and the other variables (E, I, P_b, P_t, G_b, , G_t) are non-negative. Well-posedness analysis for this model is an open problem. Main difficulties in proving existence stem when trying to find bounds for the ionic concentrations. Nevertheless simulations show that the variables seem to have the desired properties, at least with proper initial and boundary conditions. From now on we will suppose the variable to have the regularity and properties needed.

3 Numerical discretization

Let define $\mathbf{u}$ the vector of the biochemicals variables, i.e. $\mathbf{u} = [\ K_e,\ K_i,\ Ca_e,\ Ca_i,\ I,\ E,\ P_b,\ P_t,\ G_b,\ G_t]$. We rewrite the problem (eq. (5),(10), (13), (15), (16), (17) and (18)) in the following compact form:

$$\begin{cases} -\text{div}\,\mu_q(\mathbf{u})\nabla\phi = 0 \\ \rho_i(\mathbf{u})\dfrac{\partial u_i}{\partial t} - \text{div}\,\mu_i\nabla u_i + \mathbf{b}_i(\mathbf{u},\ \nabla\phi)\cdot\nabla u_i = g_i(\mathbf{u}), \quad i = 1,\ \ldots,\ 10 \end{cases} \tag{21}$$

We used different discretization for the 2D and the 3D problems. In the 2D simulations we use a fine space and time steps in order to find an accurate solution; in the 3D simulations, the goal is to get a reliable solution using larger time and space steps, avoiding the occurrence of oscillations and negative values of the concentration variables.

Discretization for the 2D simulations We discretize the evolution equations in time using a classical BDF2 scheme, while space discretization is carried out with Lagrangian finite elements, so that if $\mathbf{\Phi}$ $(\mathbf{U})$ denotes the vector of nodal values of ϕ $(\mathbf{u})$, the discrete problem reads

$$\begin{cases} \mathrm{S}_q^{n+1}\Phi^{n+1} = 0 \\ \frac{3}{2}\mathrm{M}_i^{n+1}U_i^{n+1} = \mathrm{M}_i^{n+1}\left[2U_i^n - \frac{1}{2}U_i^{n-1}\right] + \Delta t\left[\mathbf{g}_i^{n+1} - \mathrm{S}_i U_i^{n+1} - \mathrm{B}_i^{n+1}U_i^{n+1}\right], \end{cases} \tag{22}$$

where $(\mathrm{M}_i^n)_{l,k} = (\,\rho_i(U^n)\,\varphi_k,\,\varphi_l\,)$, $(\mathrm{B}_i^n)_{l,k} = \left(\,\mathbf{b}_i(U^n, \nabla\Phi^{n-1})\nabla\varphi_k,\,\varphi_l\,\right)$, $(\mathrm{S}_i)_{l,k} = (\,\mu_i\nabla\varphi_k,\,\nabla\varphi_l\,)$, $(\mathrm{S}_q^n)_{l,k} = (\,\mu_q(U^n)\nabla\varphi_k,\,\nabla\varphi_l\,)$, and $(\mathbf{g}_i^n)_l = (\,g_i(U^n),\,\varphi_l\,)$. Notice that as far as $I > I_{cr}$ hemodynamics equation is not fully coupled with the biochemical equations, and has not to be solved at each time step. To solve this nonlinear algebraic system, we use the following fixed point iteration algorithm

$$\frac{3}{2}\mathrm{M}_i^{n+1,k}\,U_i^{n+1,k+1} = \mathrm{M}_i^{n+1,k}\left[2U_i^n - \frac{1}{2}U_i^{n-1}\right] + \Delta t\,\mathbf{f}_i^{n+1,k} \quad i = 1, \ldots, 10, \tag{23}$$

for $k = 0,\, 1,\, \ldots$ with

$$\mathbf{f}_i^{n+1,0} = 2\left[\mathbf{g}_i^n - \mathrm{S}_i U_i^n - \mathrm{B}_i^n U_i^n\right] - \left[\mathbf{g}_i^{n-1} - \mathrm{S}U_i^{n-1} - \mathrm{B}_i^{n-1}U_i^{n-1}\right]$$

$$\mathbf{f}_i^{n+1,k} = \mathbf{g}_i^{n+1,k} - \mathrm{S}_i U_i^{n+1,k} - \mathrm{B}_i^{n+1,k}U_i^{n+1,k} \quad \text{for } k = 1,\, 2,\, \ldots$$

We stop the iterations when $\|\mathbf{U}^{n+1,k+1} - \mathbf{U}^{n+1,k}\| \leq \varepsilon$ and we set $\mathbf{U}^{n+1} = \mathbf{U}^{n+1,k+1}$. We resort to classical mass lumping approximations, so that M_i is diagonal, so we do solve diagonal systems at each iteration step. Alternatively, at each fixed point step we could resort to an implicit treatment of the diffusive term, requiring the solution of a non-diagonal system. However, since the diffusion coefficients are small compare to the reaction ones, this does not improve the convergence of the fixed point iterative method, as we verified in our numerical experiments.

Discretization for the 3D simulations In 3D simulations, the space and time resolutions used in the previous 2D simulations are not affordable. We still discretize in space using Lagrangian finite elements equations. In order to handle the advection dominant problems for the oxygen partial

pressure and the glucose concentration in the blood, we use the streamline-diffusion stabilization. For the time discretization we resort to a first order semi-implicit method. More precisely, we write the forcing term g_i as $g_i(\mathbf{u}) = -r_i(\mathbf{u})u_i + \overline{g}_i(\mathbf{u})$, and we solve the following discrete problem,

$$\begin{cases} \mathrm{S}_q^{n+1}\Phi^{n+1} = 0 \\ \left[\mathrm{M}_i^n + \Delta t\left(\mathrm{S}_i + \overline{\mathrm{B}}_i^n + \mathbf{r}_i^n\right)\right] U_i^{n+1} = \mathrm{M}_i^n U_i^n + \Delta t \overline{\mathbf{g}}_i^n, \end{cases} \tag{24}$$

where $(\overline{\mathrm{B}}_i^n)_{l,k} = (\,\mathbf{b}_i^n\nabla\varphi_k,\,\varphi_l\,) + \left(d^h\frac{\mathbf{b}_i^n}{|\mathbf{b}_i^n|}\nabla\varphi_k,\,\mathbf{b}_i^n\nabla\varphi_l\right)$, being $\mathbf{b}_i^n = \mathbf{b}_i(U^n, \nabla\Phi^n)$ and d^h the diameter of the current finite element; $(\mathbf{r}_i^n)_l = (\,r_i(U^n),\,\varphi_l\,)$ and $(\overline{\mathbf{g}}_i^n)_l = (\,\overline{g}_i(U^n),\,\varphi_l\,)$.
For the P_b equation, we take

$$r = \beta_b\, c_O \quad \text{and} \quad \overline{g} = \beta_b\, c_O\, P_t;$$

for the P_t equation we take

$$r = \beta_t c_O + \frac{\sigma_b\, R_{ATP}\, G_t}{6(P_t + K_O)(G_t + K_G)} \quad \text{and} \quad \overline{g} = \beta_b\, c_O\, P_b;$$

for the G_b equation we take

$$r = \frac{\beta_b\, c_G}{G_b + \overline{K}_G)} \quad \text{and} \quad \overline{g} = \frac{\beta_b\, c_G\, G_t}{G_t + \overline{K}_G)};$$

for the G_t equation we take

$$r = \frac{\beta_t\, c_G}{G_t + \overline{K}_G} + \frac{R_{ATP}}{G_t + K_G}\left(\frac{1}{2} - \frac{17}{36}\,\frac{P_t}{P_t + K_O}\right) \quad \text{and} \quad \overline{g} = \frac{\beta_t\, c_G\, G_b}{G_b + \overline{K}_G}.$$

The splitting of the forcing term in an implicit and explicit part is supposed to improve the scheme positivity properties [7]. For the other equations, the forcing term is treated in explicit ($\overline{g}_i = g_i$).

4 Numerical implementation and results

In this section, we present numerical results on 2D axisymmetric and 3D geometries. The main aim of these simulations is to provide a qualitative insight of the possible sequence of biochemical events originated by a vascular occlusion and possibly by a perfusion therapy like fibrinolysis. Simulations are carried out with the C++ library `LifeV` [2]. The 3D geometry is generated and meshed with the code Gambit [1]. The visualization and post processing of the solutions are carried out with Paraview [3] and Matlab®.

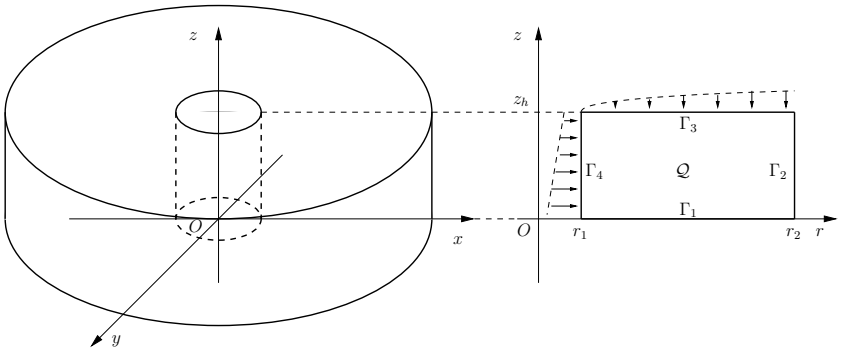

Figure 2: Axisymmetric domain: the central hole represents a vessel, the cylinder is the computational domain representing a portion of brain tissue.

4.1 Axisymmetric computation

Let us consider the geometry in figure 2 that is supposed to represent a portion of brain around an artery. We set $r_1 = 0.2\ cm$, $r_2 = 1\ cm$, $z_h = 0.5\ cm$ and $\mathcal{Q}$ is the rectangular domain having border $\partial\mathcal{Q} = \Gamma_1 \cup \Gamma_2 \cup \Gamma_3 \cup \Gamma_4$. Writing the problem in cylindrical coordinates, and imposing boundary conditions that respect the symmetry, we can solve the problem in cylindrical coordinates (denoted by $r = \sqrt{x^2 + y^2}$ and z respectively).

Initial values We prescribe the following initial conditions.

a) Potassium and calcium concentrations, energy store E and the integrity I are set to their physiological values (see table 1). In particular we set $I = 1$.

b) Blood pressure $\phi_b = \phi_b^a - \alpha(\beta - z)\ln(\gamma\, r)$ on $\mathcal{Q}$, where $\phi_b^a = 95\ mmHg$, $\alpha = 50\ mmHg\ cm^{-1}$, $\beta = 1\ cm$ and $\gamma = 5\ cm^{-1}$. In particular we assume

$$\mathbf{q} = \begin{bmatrix} q^r \\ q^z \end{bmatrix} = \begin{bmatrix} \mu_0\, \alpha\, \dfrac{\beta - z}{r} \\ -\mu_0\, \alpha\, \ln(\gamma\, r) \end{bmatrix}$$

where q^r and q^z are the radial and axial components of $\mathbf{q}$. The radial component of $\mathbf{q}$ is related to the blood coming from the artery coaxial with the cylinder and it is decreasing moving away from the artery. The axial component is related to the blood coming from other region which increases moving away from the artery. We choose $\mu_0 = 5 \cdot 10^{-5}\ dm^2\ min^{-1}\ mmHg^{-1}$. In this way we impose a flow of $0.96\ dm^2\ dm^{-3}\ min^{-1}$ which is greater than physiological cerebral blood flow in human beings, but still in the range of mammals' one (see [16]).

c) Initial values of oxygen partial pressure and glucose are the steady solutions of the system of equations (15), (16) and (17) with the following boundary conditions: $P_b = P_b^a$ on $\Gamma_3 \cup \Gamma_4$ and satisfy homogeneous Neumann condition on $\Gamma_1 \cup \Gamma_2$; $G_b = G_b^a$ on $\Gamma_3 \cup \Gamma_4$ and satisfies homogeneous Neumann condition on $\Gamma_1 \cup \Gamma_2$; P_t and G_t satisfy homogeneous Neumann condition on $\partial\mathcal{Q}$.

The computed initial values of blood pressure ϕ and velocity $\mathbf{q}$ are shown in Figure 3. Figure 4 shows oxygen partial pressure in the vessel (P_b) and in tissue (P_t), while Figure 5 shows glucose concentration in the vessel (G_b) and in tissue (G_t). Energy store (E) has the same pattern of glucose and assumes values in the range 2.2 - 2.7 mM. Ion concentrations assume values that are a slightly perturbation (less than 1%) of the resting values.

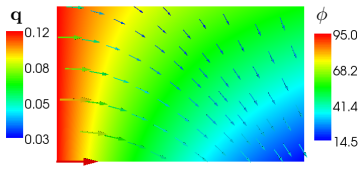

Figure 3: Initial pressure ϕ_b $[mmHg]$ and velocity $\mathbf{q}$ $[dm/min]$.

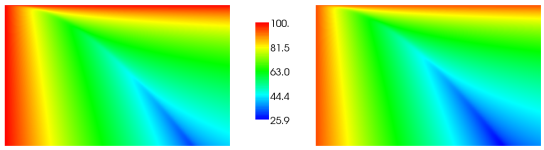

Figure 4: Oxygen partial pressure $[mmHg]$ in blood (left) and in tissue (right).

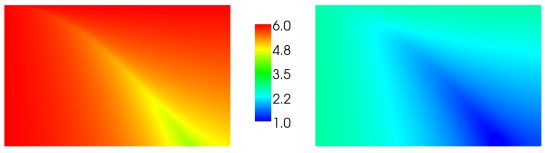

Figure 5: Glucose concentration $[mM]$ in blood (left) and in tissue (right).

Artery occlusion We study the effect of the occlusion of the central artery. To simulate this event we impose at time $t = 0$ a null blood velocity on Γ_4 (homogeneous Neumann condition), a Dirichlet condition, i.e. $\phi_b(r_1, z, t) = \phi_b(r_1, z, 0)$ on Γ_1 and on $\Gamma_2 \cup \Gamma_3$ we impose the Neumann condition $-\mu \nabla \phi_b \cdot \mathbf{n} = \mathbf{q}(r, z, 0) \cdot \mathbf{n}$. Ionic concentrations, E, I, P_t and G_t satisfy homogeneous Neumann boundary conditions on $\partial\mathcal{Q}$. P_b and G_b satisfy homogeneous boundary condition on $\Gamma_1 \cup \Gamma_2$ and the following Dirichlet condition on $\Gamma_3 \cup \Gamma_4$.

$$P_b(r, z, t) = P_b^a \left[1 + \left(1 - e^{-2t}\right)\left(r^2(3 - 2r) - 1\right)\right]$$
$$G_b(r, z, t) = G_b^a \left[1 + \left(1 - e^{-t}\right)\left(r^2(3 - 2r) - 1\right)\right]$$

We assumed that, right after the occlusion, the concentrations of oxygen and glucose in the artery and in the surrounding tissue fall down exponentially with respect to time.
The blood velocities before and right after the artery occlusion are compared in Figure 6. We notice that right after the occlusion we have only a collateral compensatory flow coming from other regions of the brain. Cells very close to the occluded artery do not receive enough blood to survive. After the stroke, oxygen partial pressure, glucose concentration and consequently the energy stores fall down. In Figure 7 we show their values at $t = 0.7$. In Figure 8 and 9 we detail in 1D the oxygen partial pressure and glucose concentrations at different time instants after the occlusion. The sharp variation in the energy store are due to the outflow of potassium from the intracellular space. As the energy decreases, in fact, the ionic pumps stop working (see first two equations in system (19)), the potassium moves from ICS to ECS and consequently the membrane potential increases. Changes in membrane potential cause changes in the membrane permeability. At the beginning we have a positive reaction and massive amount of potassium exits the cells and starts spreading through the ECS. The active pumps consumes a lot of energy trying to restore physiological potassium concentration. In Figure 10 and 11 we show intra and extracellular concentration of potassium and calcium. We can clearly distinguish two regions, one where energy is very low and the other where we still have ionic equilibrium and the Energy is almost physiologic. The first region is expanding and few minutes after the occlusion it will be characterized by necrotic tissue. This zone will become the "ischemic umbra".

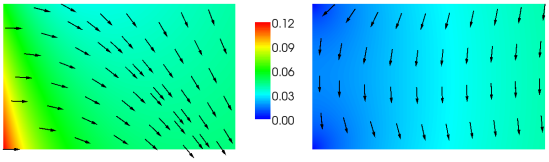

Figure 6: Velocity $\mathbf{q}\,[dm/min]$ before (left) and right after (right) the occlusion.

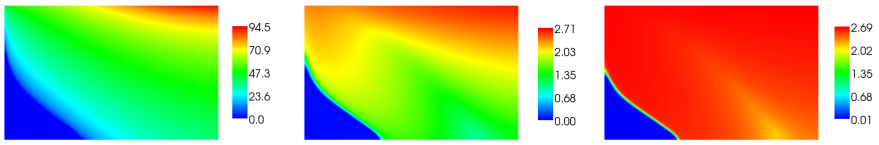

Figure 7: From left to rigth: oxygen partial pressure in tissue $[mmHg]$, glucose concentration in tissue $[mM]$ and Energy $[mM]$ at time $t = 0.7\ min$.

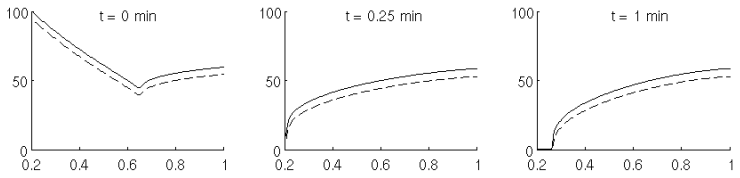

Figure 8: Oxygen partial pressures in $[mmHg]$ in blood (solid line) and in tissue (dashed line) at different time steps, along the axis $z = 0.25cm$.

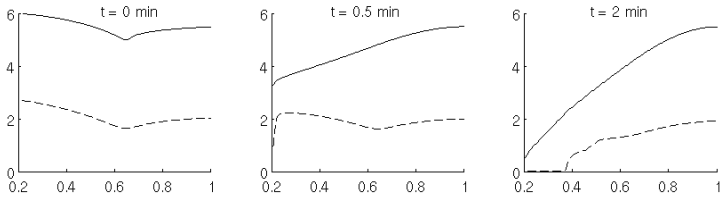

Figure 9: Glucose concentrations $[mM]$ in blood (solid line) and in tissue (dashed line) at time $t = 0.7\ min$ at different time steps, along the axis $z = 0.25cm$.

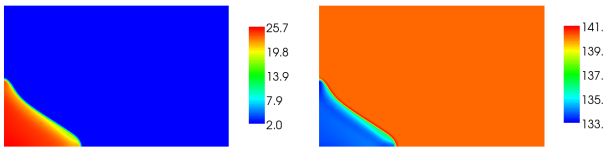

Figure 10: Potassium concentrations $[mM]$ in ECS (left) and ICS (right) at time $t = 0.7\ min$.

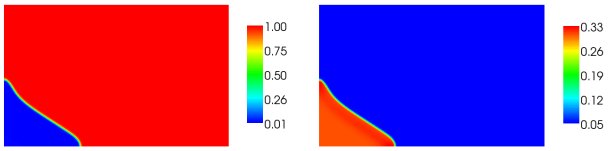

Figure 11: Calcium concentrations $[mM]$ in ECS (left) and ICS (right) at time $t = 0.7\ min$.

Extracellular potassium spreads through the ECS triggering this positive reaction even in healthy zones of tissue. In these regions ionic pumps can work properly and after a while the potassium is absorbed. This mechanism lead to the generation of SD waves, traveling waves of extracellular potassium associated with a depression in electrical activity. We now detail the "birth" of spreading depression waves. Figure 12 and 13 show the potassium concentrations at different time steps in 3D and 1D. The 1D plots are taken on the axis $z = 0.25$

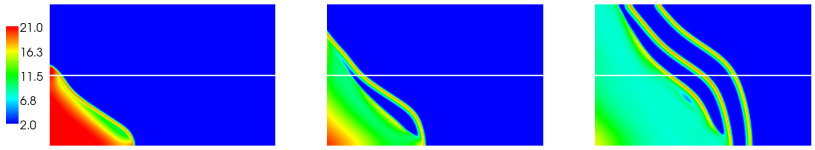

Figure 12: Extracellular potassium concentrations $[mM]$ at time $t = 0.9\ min$, $t = 1.5\ min$, and $t = 3\ min$, from left to rigth. The white line underline the axis $z = 0.25cm$ on which we plot the 1D solutions in Figure 13 and 14.

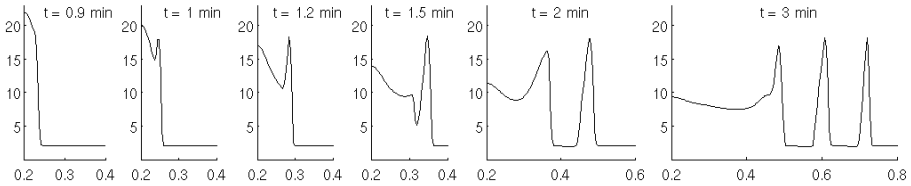

Figure 13: Extracellular potassium concentrations $[mM]$ along the radial direction at different time steps, along the axis $z = 0.25cm$.

Transmembrane potential V, potassium Nernst potential V_k and calcium Nernst potential V_{Ca} at time $t = 3\ min$ are shown in Figure 14. Notice that in the neighborhood of the occluded artery the solution is reaching an equilibrium solution, where $V_{Ca} = V$, $E = 0$ and $I = 0$.

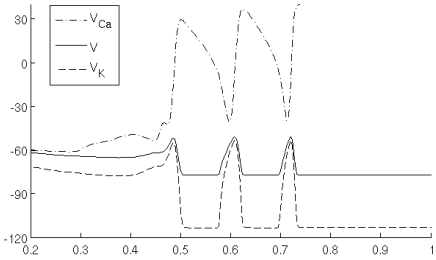

Figure 14: Radial profile of calcium Nernst potential V_{Ca}, transmembrane potential V, potassium Nernst potentials $V_K$in $[mM]$ along the axis $z = 0.25cm$.

Figure 15 shows oxygen partial pressure in the tissue, energy store and integrity 3 min after the occlusion. We notice that in correspondence with the presence of SD waves, E and mostly P_t diminish because of the increased ionic pump activity.

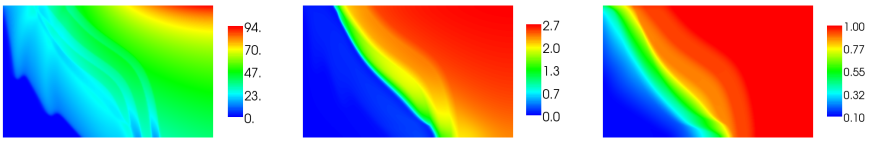

Figure 15: From left to right: Oxygen tissue partial pressure P_t in $mmHg$, Energy stores E in mM, and Integrity. All the variables are a time $t = 3\ min$

SD suppression Numerical simulations pinpoint the relevance of V_g in suppressing the SD phenomenon. This variable influences the ionic permeability of the cellular membrane (see eq. $(19)_{1,2}$). Taking $V_g = 45\ mV$, instead of 51 mV the SD phenomenon does not occur as shown in Figure 16. Comparing these pattern of K_e, E, I with the ones in Figure 12 and 15, we notice that the SD waves promote the expansion of the ischemic core. The number of SD waves observed is correlated to the size of the ischemic core (this correlation has already been observed by Ruppin et al.[33]).

Figure 16: From left: Extracellular potassium concentration in $[mM]$, energy store $[mM]$ and Integrity when SD is suppressed at time $t = 3\ min$.

Reopening of the vessel We investigate now, the effects of a new perfusion of the artery. Artery is reopen only two minutes and a half after the occlusion occurred. Figure 17 show K_e, E and I about five minutes after the occlusion, with or without reperfusion. When the tissue is reperfused the energy slowly goes back to the physiological state and impaired region, after a while, stops swelling. In the umbra region, even if the tissue is reperfused, physiological values of ions cannot be restored.
Investigating the case in which the tissue is not impaired (i.e. we set $I = 1$ and we disregard the ODE equations of integrity) we find the patterns illustrated in Figure 18, for the extracellular potassium concentrations. Here the "wave" nature of the SD phenomenon comes out, as already experimented in Tuckwell and Miura [35].

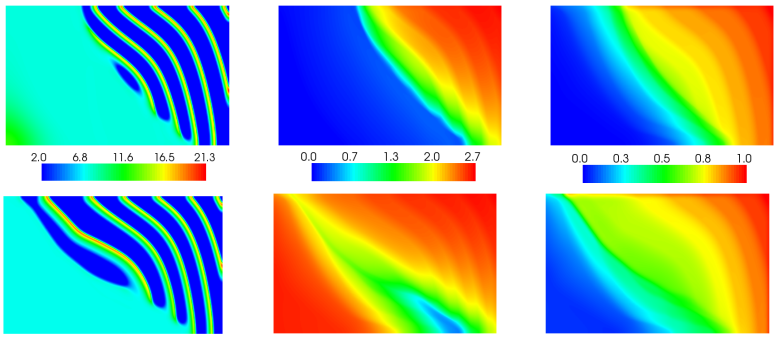

Figure 17: From top-left: extracellular potassium concentration in $[mM]$, energy store in $[mM]$ and integrity. In the bottom same variables in the reperfusion case. Time $t = 5.25\ min$.

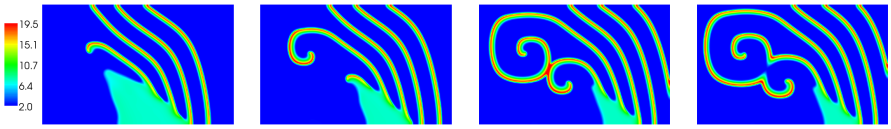

Figure 18: From left: extracellular potassium concentration in $[mM]$ at time $t = 3.8\ min$, $4.2\ min$, $4.65\ min$, $4.75\ min$ when the integrity is uncoupled.

We now perfuse the brain 5 *min* after the occlusion. Now a large part of tissue is impaired. In Figure 19 we compare the average blood velocity $\mathbf{q}$ in the physiological state with the one after the perfusion. Higher velocities point out the risk of blood leakage.

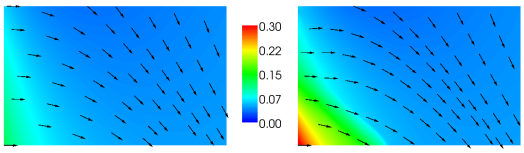

Figure 19: Velocity $\mathbf{q}\,[dm/min]$ at the initial state (left) and after (right) the perfusion at time $t = 5\ min$.

4.2 3D Simulation

We consider the geometry in Figure 20, which represents a brain portions surrounded by two arteries (in red on the left) and two veins (in blue on the left). We prescribe the following initial conditions.

a) Potassium and calcium concentrations, energy store E and the integrity I are set to their physiological values (see table 1). In particular we set $I = 1$.

b) Blood pressure ϕ_b is the solution of the system (5) with the following boundary conditions: $\phi_b = \phi_b^a$ on the artery surfaces, $\phi_b = 20mmHg$ on the vein surfaces and homogeneous Neumann condition on the remaining part of the surface. The permeability μ is taken equal to $\mu_0 = 7 \cdot 10^{-5}\ dm^2\ min^{-1}\ mmHg^{-1}$.

c) Initial values of oxygen partial pressure and glucose are the steady solutions of the system of equations (15), (16) and (17) with the following boundary conditions: $P_b = P_b^a$ on the arteries surfaces and satisfies homogeneous Neumann condition on the rest of the boundary; $G_b = G_b^a$ on the arteries surfaces and satisfies homogeneous Neumann condition on the rest of the boundary; P_t and G_t satisfy homogeneous Neumann condition on the whole external surface.

In Figure 20 we report the initial pressure ϕ_b (left) and the initial velocity $\mathbf{q}$. We notice that there are zones in which the blood velocity is almost null. This mainly depends on the particular geometry and permeability μ_0 taken. In this work we assumed μ_0 to be scalar and uniform in space. Nevertheless, the difficulties encountered in the design of a geometry which avoid hypoperfused regions put in evidence the limits of this assumption. In order to get reliable results, μ_0 should be a space-dependent tensor. This leads to the non-trivial identification of the tensor μ_0 and goes beyond the purpose of this paper.

Artery occlusion We study the effect of the occlusion of the artery on the right. To simulate this event we impose at time $t = 0$ a null blood velocity on the surface of the right artery (homogeneous Neumann condition) and the Dirichlet condition $\phi_b(\mathbf{x}, t) = \phi_b(\mathbf{x}, 0)$ on the remaining part of the external surface. Ionic concentrations, E, I, P_t and G_t still satisfy homogeneous Neumann conditions on the boundary. On the right artery surface, $P_b = P_b^a\, e^{-2t}$ and $G_b = G_b^a\, e^{-t}$; on the central artery surface, $P_b = P_b^a$ and $G_b = G_b^a$; on the rest of the boundary, we set homogeneous Neumann conditions.

The dynamics of the ischemia evolution in the simulations at hand are similar to the ones shown in the 2D simulations. The major difference is that here the phenomenon of Spreading Depression does not occur. This can be a consequence of the geometry, that does not allow triggering of the SD waves. Another possible explanation is the numerical diffusivity induced by the streamline diffusion and the time advancing methods. This point deserves further investigations, possibly resorting to a validation with real geometries. Figure 21 shows the extracellular potassium concentration

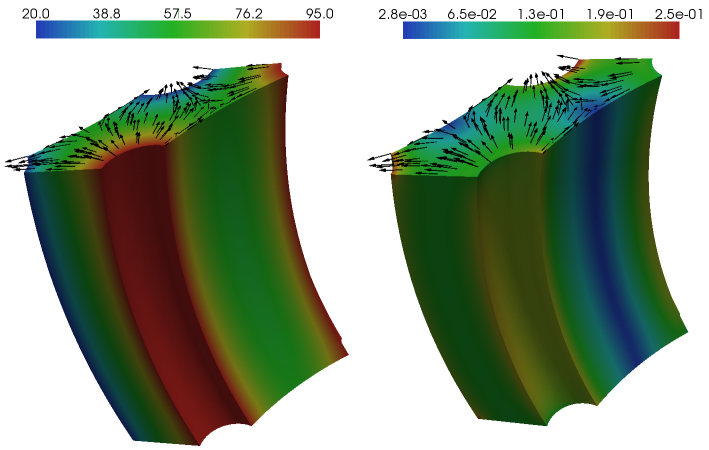

Figure 20: Left: initial pressure ϕ_b $[mmHg]$. Right: initial velocity $\mathbf{q}$ $[dm/min]$. On the top surfaces, velocity directions are shown.

K_e $[mM]$ (left) and the integrity I (right) after 15 min from the occlusion. These plots put in evidence the ischemic core region, which comes with an increase in the extracellular potassium concentration. The core region is small and this is probably a consequence of the absence of SD waves, that in general promote the expansion of the Ischemic region.

Reperfusion We now perfuse the brain 15 min after the occlusion and we compare in Figure 22 the blood velocity $\mathbf{q}$ in the physiological state and after the reperfusion. As expected, higher velocities are present in the latter case. This fact points out the risk of blood leakage when reperfusing an ischemic region.

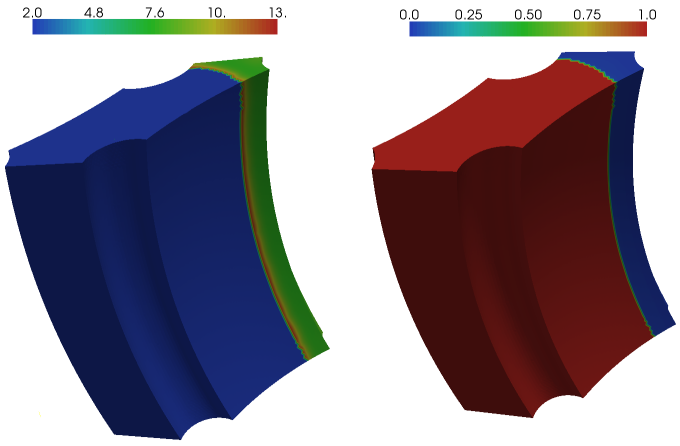

Figure 21: Extracellular potassium concentration K_e $[mM]$ (left) and integrity index I (right) after 15 min from the occlusion.

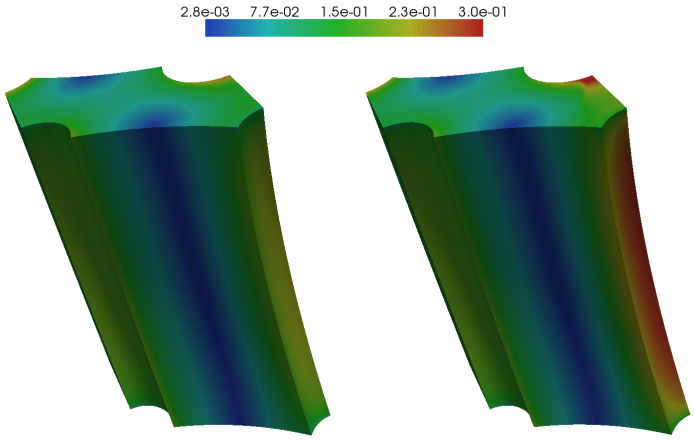

Figure 22: Velocity $\mathbf{q}\,[dm/min]$ at the initial state (left) and after (right) the perfusion at time $t = 15$ min.

5 Conclusion and Perspectives

The sequence of biochemical event induced by a reduction of blood supply in the brain is far to be completely understood. The role of BBB as an interface between hemodynamics and biochemical dynamics is currently investigated under different pathological conditions (see e.g. the recent monograph [23]). In this paper, we devised a semi-empirical mesoscale model based on homogenization of microscale dynamics, some constitutive laws for emprical indexes of clinical significance and a space-dependent description of hemodynamics. Numerical 3D results actually give interesting qualitative highlights, such as the role of V_g in suppressing the SD waves. The model proposed here is however far to be a final outcome and open many challenging problems that need to be investigated more.

1. *Validation*: quantitative validation of the model is still to be pursued, using in vivo data and real geometries. A more careful quantification of the parameters involved in the model is actually mandatory for a quantitative assessment of the reliability of the model.

2. *Analysis*: a complete well-posedness analysis of the model still needs to be carried out. The presence of different dynamics and the intrinsic nonlinearities prevented so far to have a complete analysis under realistic assumptions on the data.

3. *Numerical methods*: difficulties in the analysis reflect in challenging numerical computations, in particular for the coupling of blood and ions dynamics and the stabilization of the dominant reactive terms, forcing us to adopt small time steps. More stable and effective methods are required for an extensive validation of the model.

Along these research lines we will move our further investigations of focal ischemia.

K_e^0	2 $[mM]$	physiological extracellular potassium concentration, [35]
K_i^0	140 $[mM]$	physiological intracellular potassium concentration, [35]
Ca_e^0	0.05 $[mM]$	physiological extracellular calcium concentration, [35]
Ca_i^0	1 $[mM]$	physiological intracellular calcium concentration, [35]
I^0	1 $[adim]$	integrity of health tissue
E^0	3 $[mM]$	ATP mM in health tissue, ($2.3 - 3.1$ $[mM]$ in anaesthetized mammals, [16])
P_b^a	100 $[mmHg]$	partial oxygen concentration in arteries, [16]
G_b^a	6 $[mM]$	glucose concentration in arteries, [31]
CBF^0	0.6 $[dm^3\ Kg^{-1}\ min^{-1}]$	cerebral blood flow in man [16]
λ_b	1.13 $[adim]$	tortuosity of blood space, [17]
λ_e	1.6 $[adim]$	tortuosity of extracellular space, [9]
λ_i	3.2 $[adim]$	tortuosity of intracellular space, in [35] is put to ∞, here we take a finite value of λ to improve numerical solution regularity, without relevant loss of accuracy
λ_t	1 $[adim]$	tortuosity of tissue space, since tissue covers 97% of the domain, $\lambda_t \simeq 1$
γ	9.0 $[mM]$	parameter, [35]
δ	40 $[mM]$	parameter, [35]
D_K	$1.5 \cdot 10^{-5}$ $[dm^2\ min^{-1}]$	potassium diffusivity, [35]
D_{Ca}	$7.5 \cdot 10^{-6}$ $[dm^2\ min^{-1}]$	calcium diffusivity, [35]
D_O	$1.5 \cdot 10^{-5}$ $[dm^2\ min^{-1}]$	oxygen diffusivity, [19]
D_G	$5.4 \cdot 10^{-6}$ $[dm^2\ min^{-1}]$	glucose diffusivity, [32]
f_K	$1.17 \cdot 10^{-4}$ $[mM\ dm\ min^{-1}]$	parameter, about $-f_K/\alpha_e$ in[35]
f_{Ca}	$1.56 \cdot 10^{-6}$ $[mM\ dm\ min^{-1}]$	parameter, equals $-f_{Ca}/\alpha_e$ in [35]
r_K	10 $[mM^{-1}]$	parameter, [35]
r_{Ca}	40 $[mM^{-1}]$	parameter, [35]
p_K	7.5 $[adim]$	parameter, about $-\rho_1/\rho_2$ in [35]
g_0	$2.25 \cdot 10^{-7}$ $[mM\ dm\ min^{-1}\ mV^{-2}]$	parameter, equals $\rho_2 g_0/\alpha_e$ in [35]
p_g	0.11 $[mV^{-2}]$	parameter, [35]
V_g	51 $[mV]$	parameter, [35]
n_b^0	0.03 $[adim]$	blood porosity, [28]
n_t	0.97 $[adim]$	tissue porosity $(1 - n_b)$
n_e	0.2 $[adim]$	ECS porosity, [28]
n_i	0.77 $[adim]$	ICS porosity, $(n_t - n_e)$
α_e	$2 \cdot 10^6$ $[dm^{-1}]$	ratio between ICS membrane surface area and ECS volume, [9]
α_t	$4.12 \cdot 10^5$ $[dm^{-1}]$	ratio between ICS membrane surface area and tissue volume, $(\alpha_e n_e/n_t)$
α_i	$5.19 \cdot 10^5$ $[dm^{-1}]$	ratio between ICS membrane surface and ICS volume, $(\alpha_e n_e/n_i)$
β	1500 $[dm^{-1}]$	ratio between microvessel surface area and brain volume, (in [4] for sepia)
β_b	$5 \cdot 10^4$ $[dm^{-1}]$	ratio between microvessel surface area and vessel volume, (β/n_b)
β_t	$1.55 \cdot 10^3$ $[dm^{-1}]$	ratio between microvessel surface area and tissue volume, (β/n_t)
V_{th}	26.7 $[mV]$	RT/F, $T = 310K$
c_{IE}, c_{ICa}	4 $[mM^{-1}]$	parameters
c_{JK}, c_{JC}	10 $[adim]$	parameters
I_{cr}	0.1 $[adim.]$	value at which tissue integrity is so low that membranes are damaged and permeability increases
Ca_{cr}	0.15 $[mM\ dm^{-3}]$	value at which intracellular calcium it's so high that mechanisms that damage membrane are activated
E_{cr}	0.3 $[mM]$	value at which tissue Energy is too low to allow normal functioning of ionic pumps
H_b	8.62 $[mM]$	Hemoglobin concentration in blood [31]
h	3 $[adim]$	parameter, [31]
σ_b	$1.3 \cdot 10^{-3}$ $[mM/mmHg]$	solubility of oxygen in blood, [20]
σ_t	$1.3 \cdot 10^{-3}$ $[mM/mmHg]$	solubility of oxygen in the tissue, [20]
$\overline{O}$	0.06 $[mM]$	value of free oxygen concentration in blood at which half of hemoglobin is saturated with oxygen, [31]
c_O	0.3 $[dm\ min^{-1}]$	permeability of BBB to oxygen, $(0.0018 - 0.6$ in [20])
c_G	$2.667 \cdot 10^{-3}$ $[dm\ min^{-1}]$	"permeability" of BBB to glucose, set in order to match glucose values in [16]
K_G	0.04 $[mM]$	parameter, [31]
$\overline{K}_G$	7 $[mM]$	parameter, [30]
K_O	2 $[mmHg]$	parameter, [31]
c_Q	5 $[mM\ min^{-1}]$	energy basal supply of tissue, choosen to be 30% of total consumption at rest since 70% is used by ionic pumps, [16]
c_{ATP}	0.5 $[adim]$	ATP moli used from ionic pump to transport across the membrane 1 mole of ions, (we used the NaK pump stechiometry, 1 ATP for 2 K^+ [16])
τ_E	1 $[min]$	time constant

Table 1: Physical parameters

References

[1] *Gambit*, www.fluent.com/gambit

[2] *LifeV software*, www.lifev.org

[3] *Paraview*, http://trilinos.sandia.gov

[4] N. J. Abbott and M. Bundgaard, *Microvessel surface area, density and dimensions in brain and muscle of the cephalopod sepia officinalis*, Royal Society of London Proceedings Series B, 230 (1987), pp. 459–482.

[5] G. S. Adair, J. W. the collaboration of A. V. Bock, and H. Field, *The hemoglobin system. VI. the oxygen dissociation curve of hemoglobin*, J. Biol. Chem., 63 (1925), pp. 529–545.

[6] J. Bear, *Dynamics of Fluids in Porous Media*, Dover Publications, Sept. 1988.

[7] E. Burman and A. Ern, *Nonlinear diffusion and discrete maximum principle for stabilized galerkin approximations of the convection-diffusion-reaction equation*, Computer Methods in Applied Mechanics and Engineering, 191 (2002), pp. 3833–3855.

[8] G. Chapuisat, *Discussion of a simple model of spreading depressions*, ESAIM: proceedings, 18 (2007), pp. 87–98.

[9] L. Dai, *Lattice boltzmann equations models for migration of ions in the brain and their applications*, 1997.

[10] C. D'Angelo, *Multiscale modelling of metabolism and transport phenomena in living tissues*, PhD thesis, EPFL, 2007.

[11] U. Dirnagl, C. Iadecola, and M. A. Moskowitz, *Pathobiology of ischaemic stroke: an integrated view*, Trends in Neurosciences, 22 (1999), pp. 391–397.

[12] M. Dronne, J. Boissel, and E. Grenier, *A mathematical model of ion movements in grey matter during a stroke*, Journal of Theoretical Biology, 240 (2006), pp. 599–615.

[13] M. Dronne, J. Boissel, E. Grenier, H. Gilquin, M. Cucherat, M. Hommel, E. Barbier, and G. Bricca, *Mathematical modelling of an ischemic stroke: An integrative approach*, Acta Biotheoretica, 52 (2004), pp. 255–272.

[14] M. Dronne, S. Descombes, E. Grenier, and H. Gilquin, *Examples of the influence of the geometry on the propagation of progressive waves*, Mathematical and Computer Modelling, In Press, Corrected Proof (2008).

[15] V. Duval, S. Chabaud, P. Girard, M. Cucherat, M. Hommel, and J. P. Boissel, *Physiologically based model of acute ischemic stroke*, J Cereb Blood Flow Metab, 22 (2002), pp. 1010–1018.

[16] M. Erecinska and I. A. Silver, *Tissue oxygen tension and brain sensitivity to hypoxia*, Respiration Physiology, 128 (2001), pp. 263–276.

[17] A. Ergul, M. M. Elgebaly, M. Middlemore, W. Li, H. Elewa, J. A. Switzer, C. Hall, A. Kozak, and S. C. Fagan, *Increased hemorrhagic transformation and altered infarct size and localization after experimental stroke in a rat model type 2 diabetes*, BMC Neurology, 7 (2007), p. 33.

[18] M. Fabricius, S. Fuhr, R. Bhatia, M. Boutelle, P. Hashemi, A. J. Strong, and M. Lauritzen, *Cortical spreading depression and peri-infarct depolarization in acutely injured human cerebral cortex*, Brain, 129 (2006), pp. 778–790.

[19] J. E. Fletcher, *Mathematical modeling of the microcirculation*, Mathematical biosciences, 38 (1978), pp. 159–202.

[20] J. E. Fletcher and R. W. Schubert, *Axial diffusion and wall permeability effects in perfused capillary-tissue structures*, Bio Systems, 20 (1987), pp. 153–74.

[21] P. A. Fraser and A. D. Dallas, *Permeability of disrupted cerebral microvessels in the frog.*, The Journal of Physiology, 461 (1993), p. 619632.

[22] P. A. Fraser, A. D. Dallas, and S. Davies, *Measurement of filtration coefficient in single cerebral microvessels of the frog.*, The Journal of Physiology, 423 (1990), p. 343361.

[23] A. F. Germanò and F. Tomasello, *Blood-Brain Barrier Permeability Changes after Subarachnoid Haemorrhage: An Update: Clinical Implications, Experimental Findings, Challenges and Future Directions*, Springer, 1 ed., June 2001.

[24] J. Huyghe and D. V. Campen, *Finite deformation theory of hierarchically arranged porous solids–I. balance of mass and momentum*, International Journal of Engineering Science, 33 (1995), pp. 1861–1871.

[25] F. K. Lehner, *On the validity of fick's law for transient diffusion through a porous medium*, Chemical Engineering Science, 34 (1979), pp. 821–825.

[26] A. A. P. Leão, *Spreading depression of activity in the cerebral cortex*, Journal of Neurophysiology, 7 (1944), pp. 359–390.

[27] R. M. Miura, H. Huang, and J. J. Wylie, *Cortical spreading depression: An enigma*, The European Physical Journal - Special Topics, 147 (2007), pp. 287–302.

[28] C. Nicholson, *Diffusion and related transport mechanisms in brain tissue*, Reports on Progress in Physics, 64 (2001), pp. 815–884.

[29] K. Revett, J. A. Reggia, A. Dr, S. G. Lisberger, D. James, and A. Reggia, *Spreading depression in focal ischemia: A computational study*, the Journal of Cerebral Blood Flow and Metabolism, (1997).

[30] P. J. Robinson and S. I. Rapoport, *Glucose transport and metabolism in the brain*, Am J Physiol Regul Integr Comp Physiol, 250 (1986), pp. R127–136.

[31] M. W. Roos, *A revised mathematical model of cerebral microischemia*, Physiological Measurement, 25 (2004), pp. 1485–1493.

[32] M. W. Roos and G. O. Sperber, *A diffusion model of cerebral microischemia*, Experimental Neurology, 147 (1997), pp. 142–150.

[33] E. Ruppin, E. Ofer, J. A. Reggia, K. Revett, and S. Goodall, *Pathogenic mechanisms in ischemic damage: a computational study*, Computers in Biology and Medicine, 29 (1999), pp. 39–59.

[34] B. E. Shapiro, *Osmotic forces and gap junctions in spreading depression: A computational model*, Journal of Computational Neuroscience, 10 (2001), pp. 99–120.

[35] H. C. Tuckwell and R. M. Miura, *A mathematical model for spreading cortical depression.*, Biophysical Journal, 23 (1978), p. 257276.

[36] W. J. Vankan, J. M. Huyghe, M. R. Drost, J. D. Janssen, and A. Huson, *A finite element mixture model for hierarchical porous media*, International Journal for Numerical Methods in Engineering, 40 (1997), pp. 193–210.

[37] S. Whitaker, *Advances in theory of fluid motion in porous media*, Industrial & Engineering Chemistry, 61 (1969), pp. 14–28.